# Green preparation of high surface area Cu-Au bimetallic nanostructured materials by co-electrodeposition in a deep eutectic solvent

Elena Plaza-Mayoral[1], Paula Sebastián-Pascual[1]*, Kim Nicole Dalby[2], Kim Degn Jensen[1], Ib Chorkendorff[3], Hanne Falsig[2], María Escudero-Escribano[1]*

(1) Department of Chemistry, University of Copenhagen, Universitetsparken 5, 2100 Copenhagen, Denmark

(2) Haldor Topsøe A/S, Haldor Topsøes Allé 1, DK-2800 Kgs. Lyngby, Denmark

(3) Department of Physics, Surface Physics and Catalysis, Technical University of Denmark, Fysikvej, DK-2800 Lyngby, Denmark

*Corresponding author:

E-mail: paula.pascual@chem.ku.dk

E-mail: maria.escudero@chem.ku.dk

**ABSTRACT**

Our sustainable future requires finding new, affordable and green routes to prepare nanostructured materials used in renewable energy conversion. In this work we present an electrodeposition method in a deep eutectic solvent (DES) to prepare bimetallic high surface area nanostructures of Cu and Au with tunable structure and composition. The metal electrodeposition performed in green choline chloride within a urea deep eutectic solvent allows us to tailor the size, morphology and elemental composition of the deposits. We combine electrochemical methods with scanning electron microscopy (SEM), X-ray photoelectron spectroscopy (XPS) and energy dispersive X-ray spectroscopy (EDS) to characterize the electrodeposited nanostructured materials. We assess the increase of the electroactive surface area through the analysis of the lead underpotential deposition (UPD) on the prepared films. We observe a 5 to 15-fold increase of the active surface area compared to flat surfaces of polycrystalline Cu or Au. Our work reports, for the first time, a green route for the electrodeposition of Cu-Au bimetallic nanostructures in a deep eutectic solvent. The combination of a tailored morphology and composition with the high active surface area of the nanostructured materials make them highly promising as electrocatalysts for applications in renewable energy conversion.

**Keywords**

Electrodeposition; Surface nanostructuring; Deep eutectic solvent; Nanostructured materials; Bimetallic electrodes; Green preparation method; Active surface area

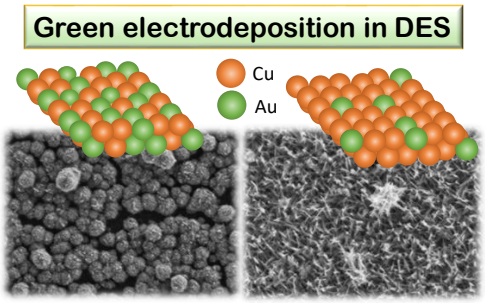


**Table of contents graphic**

## Introduction

As society continues to move towards a carbon-free economy, there is an increase in the urgent demand to produce more efficient nanotechnologies for clean energy conversion.[1,2] During the past decade, the scientific community has dedicated substantial efforts to design novel nanocatalysts for a variety of applications such as energy conversion and storage, as well as sustainable electrosynthesis processes, necessary in the green energy transition.[3–6] In this regard, developing new methods and strategies for controlled preparation of tailored nanostructured materials, in an environmentally friendly manner and without compromising its competitiveness, is crucial to decarbonize the industry.[1,2]

Chemical synthesis of nanoparticles usually employs colloidal routes in which different surfactant agents or templates are necessary to guarantee crystallinity of the nanoparticles.[7] The methods required to remove the surfactant agent, which poisons the catalyst surface and affects its catalytic performance.[8,9] Physical methods, such as sputtering from metallic-targets and in ultra-high vacuum conditions, allow for the controlled preparation of multimetallic nanoparticulate thin films, although at the expense of high energy consumption.[10] In recent years, electrodeposition of metallic nanostructures in green organic solvents has been proposed as a sustainable alternative for the synthesis of new materials.[11–13] Electrodeposition is a versatile and relatively inexpensive

technique for tuning the deposition of different metallic alloys and metal oxides.[14] Tailored morphology and composition is obtained by simply fine-tuning certain parameters, such as applied potential conditions and composition of the electrodeposition bath, which contains the electrolyte and the metal precursors.[12] Traditionally, electrodeposition was performed in aqueous solutions and in the presence of additives, to facilitates the reduction of metals with very negative reduction potentials, while avoiding the interference of the solvent co-reduction.[15,16] Alternatively, deep eutectic solvents (DES) have been suggested as ideal candidates for green electrodeposition of nanostructures.[17,18] Formed by the eutectic mixture of a quaternary ammonium salt and a neutral proton donor, they provide wide potential limits, enough conductivity and usually do not require the use of additives.[19] The single electrodeposition of a majority of metals has been successfully conducted in DES.[12,20–24] However, electrodeposition of noble bi- or multimetallic nanostructures in DES has not been fully explored.[25–29]

While monometallic nanostructures with variable shape and sizes have been extensively investigated for different electrocatalytic reactions,[30–32] new bimetallic and multimetallic nanostructures continue to emerge.[33–35] When two or more metals are combined, the aim is to enhance the catalytic performance towards desirable compounds in different electrocatalytic reactions, by tuning the electronics of the multimetallic surface.[4,36] Among other bimetallic catalysts, the Cu-Au system presents interesting properties for a variety of reactions, including the oxidation of CO[37], electrochemical and photoelectrochemical hydrogen evolution reaction[38,39], design of non-enzymatic biosensors,[40] and electroreduction of $CO_2$ into fuels and CO.[41–44] Developing clean approaches to selectively tailor morphology, shape and size of multimetallic materials is, thereby, relevant in order to design efficient catalysts for different applications.[3,4,45,46]

In addition to the improved catalytic properties when combining two or more metals, nanostructured substrates usually display enhanced electrocatalytic activities (per mass unity of catalyst) compared to flat or bulk electrodes.[47,48] This is, among other reasons, because of their high electrochemically active surface area (ECSA), which accounts for the total number of reaction sites versus geometric area of surface catalyst.[49–52] In this work, we present an alternative methodology to prepare bimetallic structures of Cu and Au with high extended surface area, via metal co-electrodeposition in choline chloride plus urea deep eutectic solvent. A glassy carbon electrode was selected as deposition substrate due to its low activity towards the reduction of the DES, thus providing a wide potential window of around 4 V.[53,54] Cyclic voltammograms (CVs) and chronoamperometric curves were recorded to clarify the co-deposition mechanism and to establish the best potential conditions for the preparation of the bimetallic films. Ex-situ field emission scanning electron microscopy (FE-SEM), energy dispersive X-ray spectroscopy (EDS) and X-ray photoelectron spectroscopy (XPS) were used to assess the morphology, composition and distribution of Au and Cu in the nanostructured deposits. The co-electrodeposition of Cu and Au was conducted using two baths with different concentrations of Au and Cu salt precursors, to tailor the structure, composition and morphology of the bimetallic nanostructures. Finally, we analyzed the ECSA by means of lead underpotential deposition (Pb UPD) on the prepared films. Pb UPD on metallic surfaces is a surface process sensitive to the structure and area of the catalyst which allows for more reliable quantification of the electroactive surface area.[55]

## 1. Experimental section

Choline chloride (ChCl, Across organics, 99%) and urea (Sigma-Aldrich, 99%) were purchased at the highest available purity. The DES was prepared by mixing both choline chloride and urea salts in a 1:2 molar ratio and under constant stirring at 40ºC. De-hydrated $AuCl_3$ and $CuCl_2$ salts were

similarly purchased (Sigma-Aldrich, 99%). To prepare the different bath-solutions employed in this work, specific amounts of $AuCl_3$ and $CuCl_2$ salts were dissolved in the DES under magnetic stirring, vacuum and heating conditions ($T$<60ºC) overnight. Two bath solutions were prepared and tested in this work: i) a 0.05 M $CuCl_2$: 0.05 M $AuCl_3$ + DES solution, i.e., Cu and Au 1:1 molar ratio solution; ii) a 0.075 M $CuCl_2$: 0.025 M $AuCl_3$ + DES solution, i.e., Cu and Au 3:1 molar ratio solution. Ultra-pure perchloric acid, potassium perchlorate (Merck, Suprapur®, 99.995 % purity) and lead (II) perchlorate hydrate (Sigma-Aldrich Merck, 99.995% of purity) were purchased to prepare a 2 mM $Pb(ClO_4)_2$ + 0.1 M $KClO_4$ + 1 mM $HClO_4$ employed for the Pb underpotential deposition.

The working electrodes were a glassy carbon (GC) rod ($Ø$=0.1963 $cm^2$), a polycrystalline Cu rod ($Ø$=0.2826 $cm^2$) and a polycrystalline Au bead electrode (0.183 $cm^2$), prepared following the Clavilier's method.[56] For the pre-treatment of the electrodes, the glassy carbon was polished until mirror finish using water-based α-alumina powder of 0.3 µm and 0.05 µm coarseness (Struers). After polishing the glassy carbon rod, the electrode was sonicated in milli-Q (18.2 MΩcm, TOC<5 ppm) water for 1 minute, and dried with a nitrogen stream before the electrodeposition. The Cu(poly) rod electrode was polished with α-alumina (0.3 µm) and, then, electropolished in a $H_3PO_4$ plus $H_2SO_4$ plus water solution with a volume ratio of 10:3:1, respectively. The gold bead electrode was pre-treated by flame-annealing and cooled down in air. The electrochemical measurements were carried out with the Cu and GC disks in the meniscus configuration while the Au bead was immersed into the solution.

The electrochemical experiments were performed in a three-electrode cell configuration using a Bio-Logic potentiostat. The metal electrodeposition in DES was performed in a thermostated small-volume (25mL) electrode cell. Copper wires for single deposition of copper, and gold wires

for the deposition of gold and Cu-Au bimetallics were used as both quasi-reference and counter electrodes. Potential values in the electrodeposition process, were referred to the Ag|AgCl reference electrode scale. The temperature was kept at 70ºC in all experiments carried out in DES solutions. For the voltammetric analysis in aqueous solution and at room temperature, a classical standard three-electrode cell was employed. A saturated calomel electrode (SCE) from Crison was used as a reference electrode and placed in a Lugging capillary. The counter electrode was a gold wire in case the deposits were composed by gold or gold-copper mixtures, and a copper wire was used for the analysis of the pure copper deposits.

The morphology of the samples was analyzed using the high-resolution Zeiss Gemini 500 field emission scanning electron microscope at Haldor Topsøe S/A. An Inlens and SE2 detector were used at low voltage (2 keV) to take high resolution images with the FE-SEM. Higher voltages (15 kev) were then used when collecting energy dispersive X-ray (EDS) data. The EDS was performed using a Thermo Scientific UltraDry silicon drift detector and processed using Pathfinder Software. All XPS measurements were conducted by a Theta Probe instrument (Thermo Scientific) using an Al anode X-ray source ($K_\alpha$ line = 1,486.6 eV). The XPS chamber's base pressure was between $8.0\times10^{-9}$ and $5.0\times10^{-10}$ mbar. The X-ray beam size was 400 μm and the pass energy utilized was 100 eV. Before the ex-situ morphological characterization, the samples were cleaned with milli-Q water at near 90 ºC, in order to remove the remaining DES on the surface.

## 3. Results and discussion

### 3.1. Single Au deposition and Cu deposition

Before studying the co-deposition of gold and copper, we assessed the gold and copper single electrodeposition on glassy carbon. Cyclic voltammograms (CVs) as well as chronoamperometric curves at different applied potentials, were recorded for either Cu and Au single electrodeposition

in DES, aiming to establish the optimal potential range at which each single metal deposits. The CVs as well as the recorded chronoamperometric transients appears in Figure S1 of the supporting information (S.I.), with our results being in line with previous reports.[23,24] The S.I. also contains the detailed description of the experimental voltammetric and chronoamperometric curves. The morphology aspect of the prepared Au and Cu single deposits in DES was assessed by using FE-SEM. Figure 1A shows the FE-SEM images of the gold deposit performed at a moderate overpotential of -0.45 V vs Ag|AgCl and after reaching a charge of -25 mC. Flower-shaped gold nanoparticles (NPs) with a diameter of ca. 300 nm are formed. This morphology is likely induced by the particle agglomeration promoted by a high surface diffusion on the GC substrate. All gold NPs display a similar shape and size. Figure 1B shows the FE-SEM image of a less covered sample prepared at -10 mC of circulated charge. The gold nanoparticles have the same flower-shape but show a lower degree of agglomeration and more pristine areas of exposed GC surface.[23] These results are in line with studies carried out by *Lu Wei et al.*[24] at short times of deposition. EDS analysis (Figure S2B) confirmed the presence of gold. Figure 1C shows the FE-SEM images of the copper deposit performed at a moderate overpotential of -1.1 V vs Ag|AgCl and after circulating a charge of -25 mC. Under these conditions, nanostructured copper plates with a triangle shape are formed, showing that the particular composition of the DES induces a specific morphology on the Cu deposits. A less covered deposit of -10 mC prepared at -1.0 V vs Ag|AgCl (Figure 1D) displays rounded copper nanoclusters ranging between 300 and 500 nm of diameter.[57] These rounded nanoparticles are likely the precursors to form the singular triangular plated morphology in Figure 1C at longer deposition times. In addition, no formation of dendrites is observed at lower magnification (Figure S3A and B). The presence of pure copper was confirmed by EDS analysis (Figure S3C).

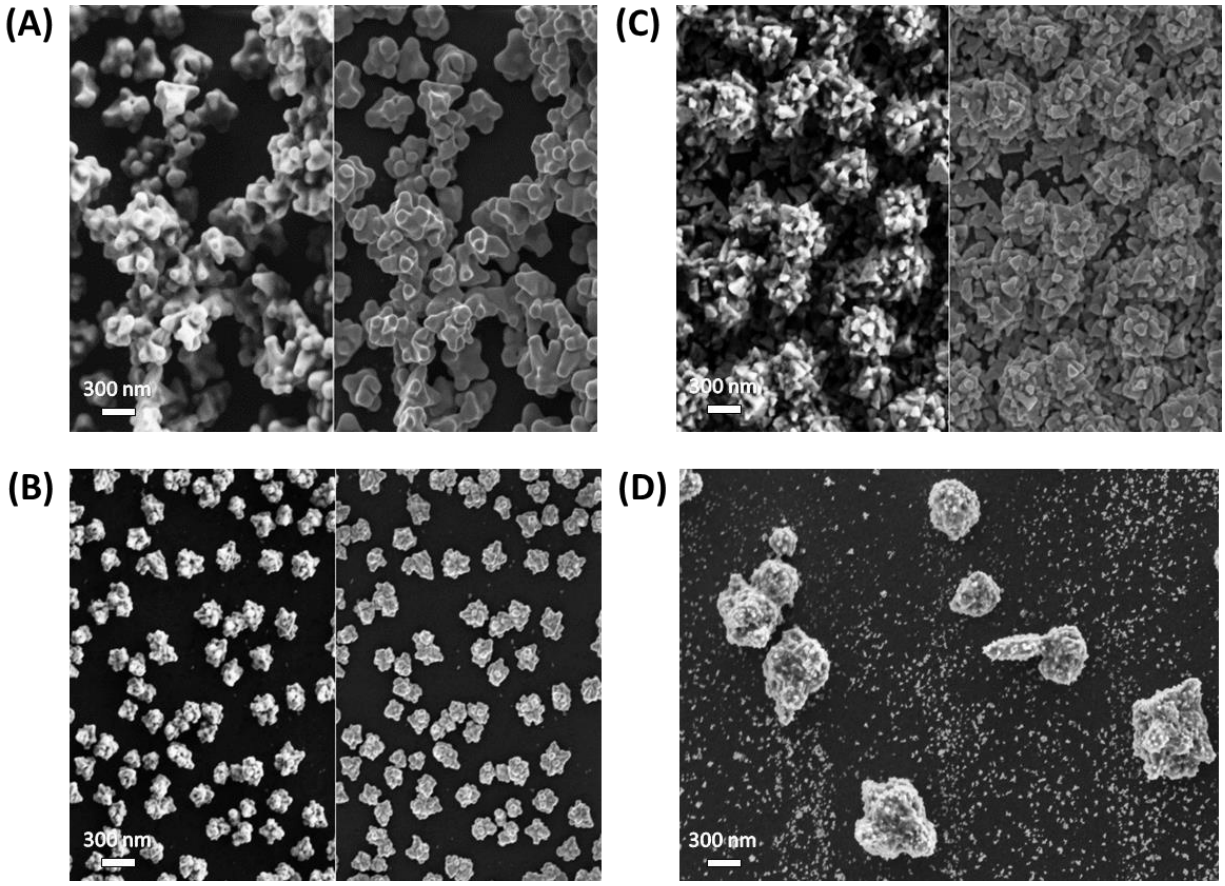


**Figure 1.** FE-SEM images of **(A)** a gold deposit prepared at -0.45 V vs Ag|AgCl, *Q*=-25mC; **(B)** a gold deposit prepared at -0.45 V vs Ag|AgCl, *Q*=-10mC; **(C)** copper deposit prepared at -1.1 V vs Ag|AgCl, *Q*=-25mC; **(D)** copper deposit prepared at -1.1 V vs Ag|AgCl, *Q*=-10mC. Split screen with SE2 detector images on the right and Inlens detector images on the left. All images have a HFW of 5 µm, a 2.3 mm WD and were taken at 2 keV.

### 3.2. Bimetallic Cu-Au nanostructures

After analyzing the single deposition of Au and Cu on GC, we performed the co-deposition of both metals from a 0.05 M $AuCl_3$: 0.05 M $CuCl_2$ + DES solution (molar ratio between Cu and Au of 1:1) at 70 ºC. Figure 2A shows the CVs of the Au and Cu co-deposition at different cathodic

potential limits. Figure 2A**,** curve a) shows the shortest potential window between -0.55 V and 1.05 V vs Ag|AgCl. In this potential window, a reduction current starting at -0.35 V vs. Ag|AgCl is observed until peak II is reached, which corresponds to gold electrodeposition. The counter-oxidation peak (peak II') overlaps with the characteristic feature related with the first $Cu^{2+}$ to $Cu^{1+}$ electron transfer (peaks I-I').[58] The absence of the characteristic oxidation peak of metallic Cu corroborates, as expected, that gold deposition occurs prior to the onset of Cu deposition in the Cu and Au 1:1 molar ratio solution. Enlarging the cathodic potential limit progressively from -0.55 V to -1.05 V vs Ag|AgCl (curves b), c) and d) in Figure 2A) causes the appearance of a third reduction peak (peak III) most likely involving both Cu and Au co-electrodeposition. Consequently, a broad $Cu^{0}$ to $Cu^{1+}$ oxidation peak between -0.1 V and -0.3 V vs Ag|AgCl has emerged (peak III'), while the oxidation peak of gold increased in intensity (peak II'). The intensity of the gold oxidation peak is considerably higher than the metallic Cu oxidation peak, suggesting that, for the Cu and Au 1:1 solution and selected potential range, the Au contribution in the co-deposition process is higher. Chronoamperometric transients were recorded at different applied potentials (Figure 2B). The *j-t* transients only display a single maximum current peak rather than multiple peaks, and the current curves practically overlaps (Figure 2B) at longer times, which could be an indication that both Cu and Au co-nucleate and growth.

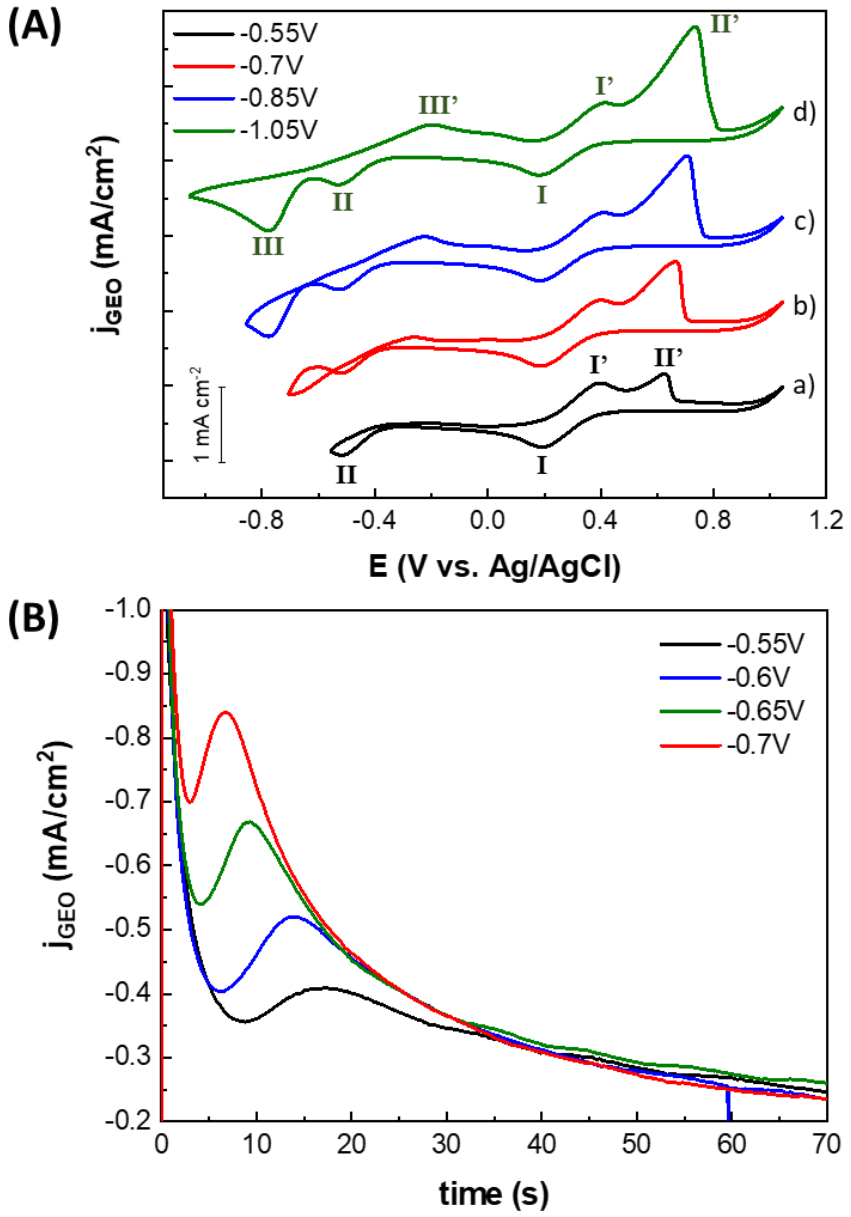


**Figure 2.** Electrodeposition in 0.05 M $CuCl_2$: 0.05 M $AuCl_3$ + DES solution at 70 ºC on a glassy carbon electrode: **(A)** cyclic voltammograms at 50 mV/s and different potential limits of **a)** -0.55 V, **b)** -0.7 V, **c)** -0.85 V, **d)** -1.05 V vs Ag|AgCl; and **(B)** *j-t* transients at different potentials of -0.55 V (black line), -0.6 V (blue line), -0.65 V (green line) and -0.7 V (red line) vs Ag|AgCl.

The analysis of the morphology of a Cu-Au bimetallic nanostructured electrode from the 1:1 molar ratio bath solution was assessed by FE-SEM. Figure 3A shows the FE-SEM image of a Cu-Au sample prepared at -0.72 V vs Ag|AgCl and under stationary conditions. Rounded nanoparticles were formed with a diameter below 300 nm and with needles or spines emerging from the surface. Additionally, the nanoparticles are homogenously distributed across the entire surface (Figure 3A, left panel). Cu-Au bimetallic samples were also prepared at slightly lower applied potential (at -0.69 V vs Ag|AgCl), but under stirring conditions (200 rpm) in order to increase the mass diffusion. Figure 3B shows the morphology of the new Cu-Au sample, which displays slightly bigger rounded nanoparticles than in Figure 3A. The rounded nanoparticles are also homogeneously distributed and cover the entire surface (Figure 3A and 3B, left panels). These rounded nanoparticles also displayed similar morphology to those prepared with no stirring, showing small spines on top of the NPs, which indicates that stirring conditions have little effect on the morphological aspect. This generated morphology is clearly different than the morphology of either pure deposited Au or Cu in DES (Figure 1). These results suggest that tuning the applied potential allows both Au and Cu to grow forming the bimetallic structure. The EDS colour maps of Cu (purple) and Au (red) elements in Figure 3C, verifies the presence of Au and Cu in the sample. The EDS analysis of the abundance of the elements in the sample (Figure S4A and B) indicates that the mass relation between Au and Cu is 2:1, respectively. However, EDS results are only semi quantitative This would imply a molar ratio of approximately 1:1 for Au and Cu in the bimetallic structure.

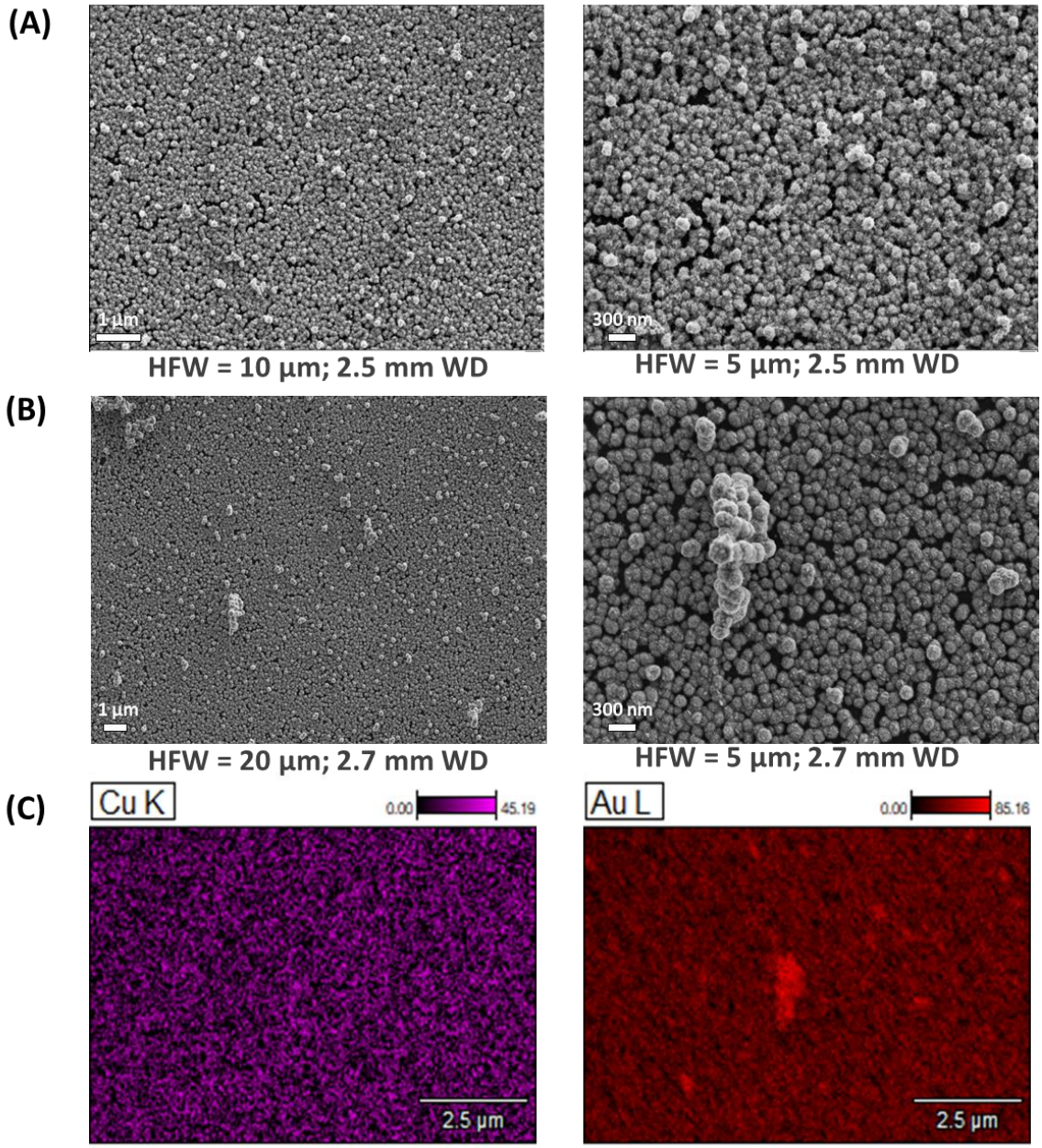


**Figure 3.** FE-SEM images of Cu and Au co-deposited nanostructures obtained from electrodeposition in 0.05 M $CuCl_2$: 0.05 M $AuCl_3$ + DES solution on glassy carbon and after circulating a charge of -25 mC: **(A)** at -0.72 V vs Ag|AgCl and stationary conditions **(B)** at -0.69 V vs Ag|AgCl and stirring at 200 rpm. Right and left panels correspond to the FE-SEM of the same samples but different magnification. **(C)** EDS maps (in wt%) of the co-deposited Cu and Au content in sample **(B)**.

Aiming for a higher Cu content in the bimetallic nanostructures, the concentration of copper in DES was increased. Figure 4A illustrates the CVs of Cu and Au co-deposition at different potential limits, and from a solution containing 0.075 M $CuCl_2$: 0.025 M $AuCl_3$ in DES, i.e, with a 3:1 molar ratio of Cu and Au. The 3:1 molar ratio metallic solution shows the same voltammetric features as those that were obtained in the 1:1 molar ratio solution. As expected, peak III´, which is related with the oxidation of the deposited Cu, is more intense due to the higher amount of copper deposited in this bath-solution. Figure 4B illustrates the corresponding 3-D nucleation and growth chronoamperometric transients at different applied potentials. Similar to the results in Figure 2B, the curves present a good overlapping at longer times. The *j-t* transients display a profile more similar to those for single Cu electrodeposition (FigureS1D), which suggests a major contribution of copper in the formation of the film when the Cu and Au 3:1 solution is used.

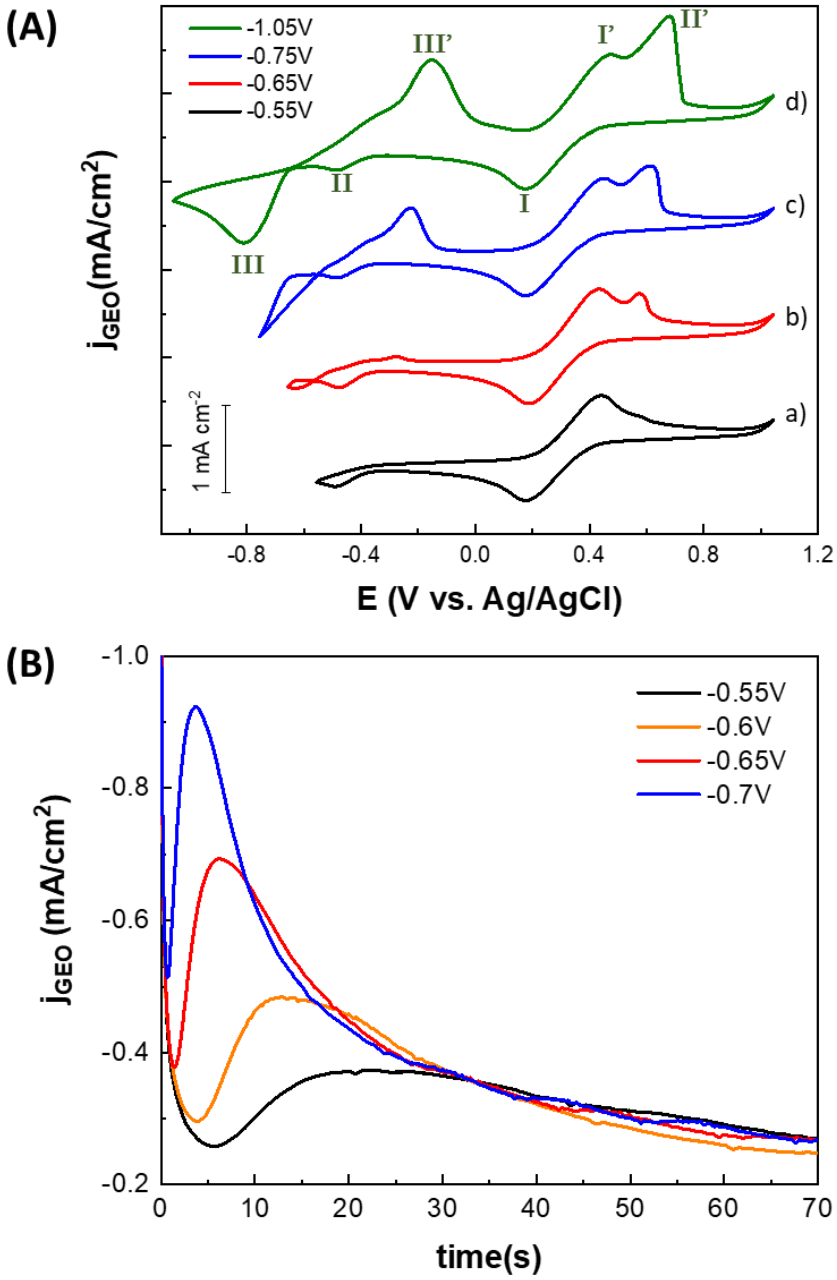


**Figure 4.** Electrodeposition in 0.075 M $CuCl_2$: 0.025 M $AuCl_3$ + DES solution at 70 ºC on a glassy carbon electrode; **(A)** cyclic voltammograms at 50 mV/s and different potential limits (-0.55 V, -0.65 V, -0.75 V, -1.05 V vs Ag|AgCl; and **(B)** *j-t* transients at different potentials of -0.55 V (black line), -0.6 V (orange line), -0.65 V (red line) and -0.7 V (blue line) vs Ag|AgCl.

FE-SEM samples were prepared at moderate overpotential to investigate the morphology of the obtained nanostructured films under these conditions. Figure 5A contains the FE-SEM images of the Cu and Au co-deposition on GC from the 3:1 molar ratio solution at -0.65 V vs Ag|AgCl, -25 mC of circulated charge and under stationary conditions. The obtained co-deposited nanostructured electrode displays the formation of a network with tiny spines in which the rounded shape has completely disappeared. In Figure 5B, the Cu-Au bimetallic obtained from the 3:1 bath solution was carried out at the same applied overpotential, i.e, at -0.65 V vs Ag|AgCl, but after decreasing the circulated charge to -18 mC. This sample still shows a high population of spines or needles but in which, unlike in Figure 5A, clusters of 300nm can be differentiated. The EDS analysis confirmed the presence of both Cu and Au homogeneously distributed over the surface (Figure 5C). The semi-quantitative chemical analysis obtained from the EDS shows the highest amount of Cu in any of the samples prepared from the 3:1 molar ratio solution (Figure S5). The wt% content of Cu in the sample prepared at -25 mC (Figure S5A) is approximately double than Au. This implies a molar relation between Cu and Au of 5:1 in bulk structure. However, the EDS analysis also evidences a lower Cu mass content in the sample prepared at -18 mC (Figure S5B). The mass content of Cu is 1.5 times higher than Au in this sample, which would be equivalent to a molar ratio between Cu and Au of 4:1, respectively. These results clearly evidence that increasing the content of copper in the bimetallic film, causes the loss of the rounded shape morphology obtained in the 1:1 bath solution, and enhances the growth of spines.

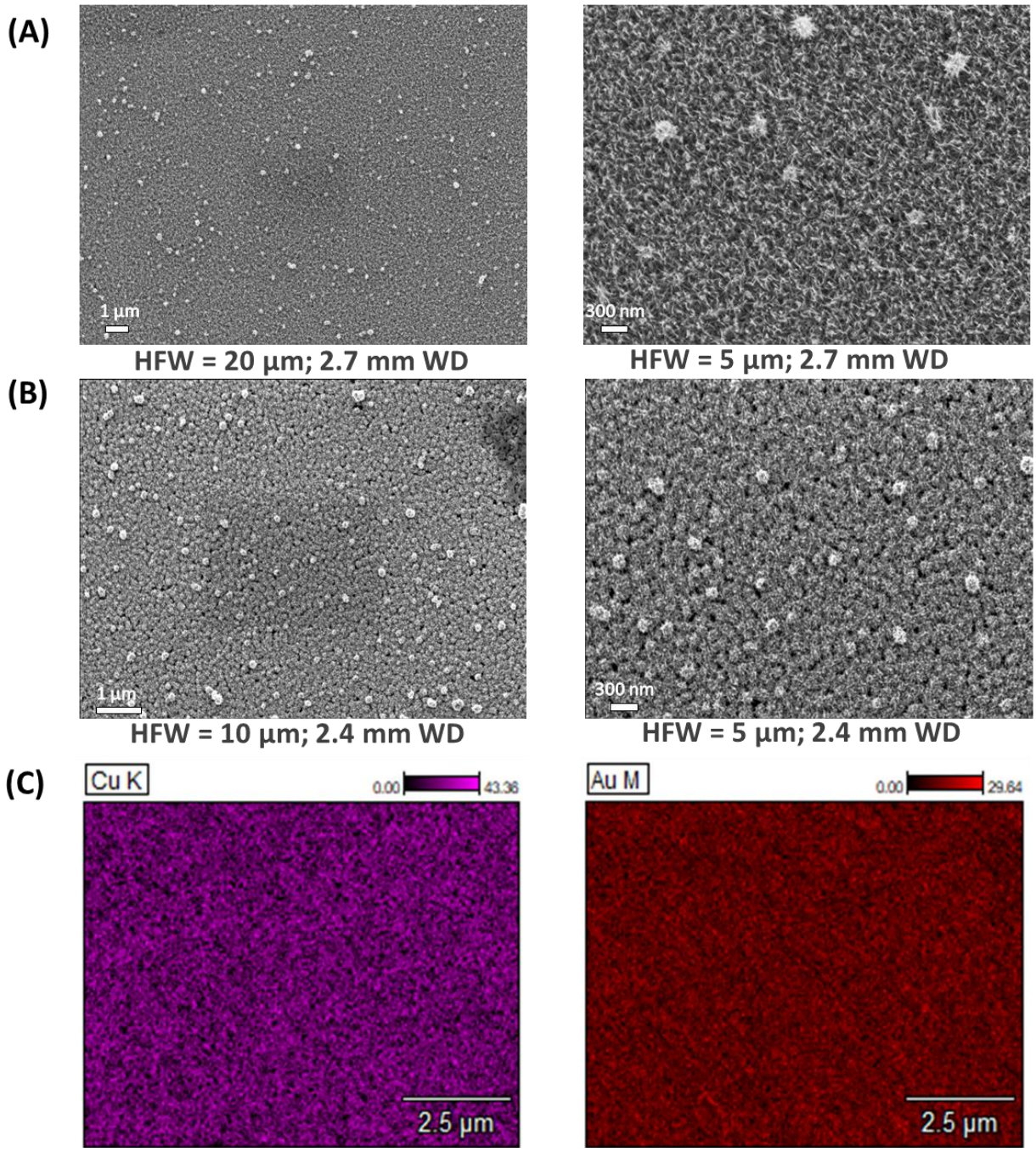


**Figure 5.** FE-SEM images of Cu and Au co-deposited nanostructures obtained from 0.075 M $CuCl_2$: 0.025 M $AuCl_3$ + DES solution on glassy carbon at -0.65 V vs Ag|AgCl, under stationary conditions and different circulated charges: **(A)** at -25 mC, **(B)** at -18 mC. **(C)** EDS analysis (in wt%) of the co-deposited Cu and Au content in sample **(B)**.

To investigate the chemical composition and chemical states of the elements at the surface layers of the prepared deposits, XPS analysis was conducted. Figure S6 shows the XPS data of the bimetallic deposits prepared in Figure 3A and 5B. The Cu *2p* and Au *4f* spectra were recorded for each Cu-Au sample, which confirmed the presence of both elements in the bimetallic films. Details of the XPS spectra are provided in the S.I. of this paper. Interestingly, the intensity of the $Au_{4f}$ peaks are substantially low, particularly in samples prepared using the Cu and Au 3:1 bath-solution in which they are almost negligible. A plausible explanation to this behavior is that, Au deposition occurs at lower applied potential than Cu (Figure S1), thereby activating the Cu electrodeposition, which would be deposited on top of Au. The increase of Cu at the surface in relation to Au is especially accentuated at the samples prepared from the DES solution with higher content of Cu salt precursor, i.e. using the Cu and Au 3:1 solution. However, since the XPS measurements have been conducted *ex-situ*, it is also very likely that the elements in the surface have redistributed because of the oxidation of Cu by exposure of the sample to air (see S.I).

In summary, results obtained by the ex-situ characterization analysis suggest that higher concentrations of gold in the bimetallic Cu-Au film induces the formation of rounded discrete nanoparticles. This rounded morphology is lost as the content of copper increases, which enhances the agglomeration of the particles and induces the formation of spines or needles. The ratio between Au and Cu in the bimetallic film dramatically affects the morphological aspect of the deposits with an increase of Cu in the more superficial layers.

### 3.3 Electrochemical determination of the electroactive surface area

Electrochemical characterization of the Cu-Au films was conducted by recording the blank cyclic voltammograms in 0.1 M sodium bicarbonate solution (Figure S7), and in the oxide region up to

1.1V vs SHE. The voltammetric features in the oxide region are clearly affected by the relative content of Cu and Au in the film. Rising the Cu content causes that the oxide reduction peaks split and shift to more negative potential values compared to the gold oxide reduction peak, approaching to the CV of pure Cu. These results agree with the previous one reported by *Liu et al.*, showing that the method allows preparing clean bi-metallic surfaces of Cu and Au[43] To assess the ECSA of the prepared co-deposited films, lead underpotential deposition (Pb UPD) on the nanostructured bimetallic films was evaluated. Underpotential deposition is the reversible deposition of a submonolayer or monolayer of a foreign element onto the substrate, at potentials more favorable than the thermodynamic reduction potential of this element. Pb UPD is, thereby, a surface process sensitive to the structure and active area of the catalyst.[55] To calculate the ECSA of the prepared films, we have integrated the charge (in micro coulombs, μC) involved in the cathodic voltammetric curve of the Pb UPD recorded on each Cu-Au sample (Figure 6).[59] The integrated charge values were normalized by the geometric area of the glassy carbon substrate to obtain the surface charge density or surface charge area values of the nanostructured films ($\mu C/cm^2$). These integrated charge values were divided by the average value between the theoretical surface charge densities ($\mu C/cm^2$) of both Au and Cu polycrystalline flat surfaces, to assess the increase in effective area or roughness factor (R) of the nanostructured films. Polycrystalline Au and Cu electrodes are flat surfaces, i.e., their roughness factor is equal to 1 (R=1). This means that the geometric area of the electrode correlates with its electroactive surface area in these surfaces.[59] In the case of the prepared high surface area nanostructures, the roughness factor (R) provides the relation between the effective electroactive surface catalyst area (ECSA) and the geometric area ($A_{GEO}$) of the employed glassy carbon substrate.[60]

Figure 6A shows the CVs of the Pb UPD on copper (red line) and gold (black line) flat polycrystalline electrodes. The calculated surface charge areas of both Cu and Au polycrystalline electrodes approach to 300 μC/cm$^2$, in agreement with the literature.[59] Thereby, we have assumed that the surface charge area of a Cu-Au film with R equal to 1 likely approaches to 300 μC/cm$^2$. Pb UPD on the Cu-Au co-deposits prepared from either the 1:1 molar ratio solution (Figure 6B) and the 3:1 molar ratio solution (Figure 6C), are compared with Pb UPD on polycrystalline Cu and Au flat surfaces. Figure 6B clearly shows a strong increase of the current density values of the Pb UPD on the deposited Cu-Au bimetallic nanostructures, after normalizing them with the geometric area of the glassy carbon substrate. The integrated charges from the Pb UPD CVs and calculated ECSAs as well as the R for the prepared deposits, are summarized in Table 1. The obtained roughness factors (R) range between 5 to 15, revealing an increase of the active surface area 5 to 15 times higher than the geometric surface area. Based on our results we conclude that preparation of nanostructured bimetallic Cu-Au films through metal electrodeposition in green deep eutectic solvents, generates material with high extended surface areas which ultimately will cause an increase in the electrochemical activity.

**Table 1.** Calculated charges of the Pb UPD in the prepared samples. Determination of the roughness factor (R) and the ECSA. The geometrical area ($A_{GEO}$) corresponds to the geometric area of the employed glassy carbon substrate which is 0.19625 cm$^2$.

| *Molar ratio Cu(II):Au(III) in DES* | *Surface charge/$A_{GEO}$ (μC/cm$^2$)* | *R= ECSA/ $A_{GEO}$* | *ECSA (cm$^2$)* |
|---|---|---|---|
| 1:1 | 4148 ± 200 | 13.8 | 2.71 ± 0.13 |
| 3:1 | 1637 ± 220 | 5.45 | 1.07 ± 0.15 |

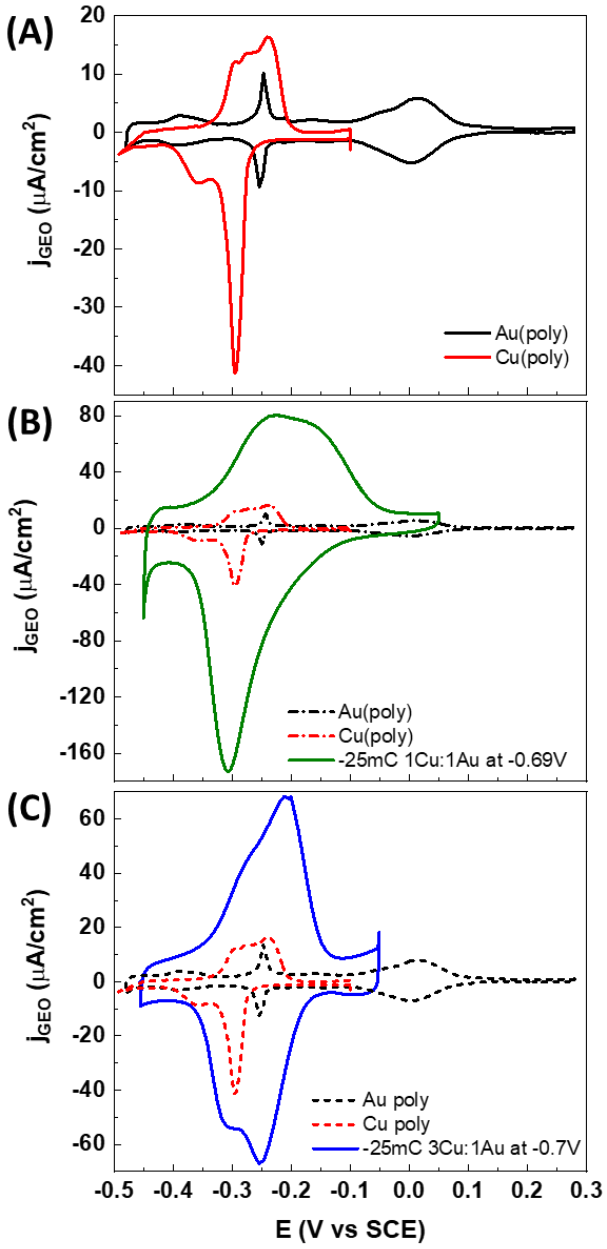


**Figure 6.** Cyclic voltammetry showing the UPD of Pb in 0.1 M $NaClO_4$ and 2 mM $Pb(ClO_4)_2$ for **(A)** polycrystalline gold (black line) and a polycrystalline copper (red line) electrodes; and Cu and Au co-deposits of **(B)** -25 mC of circulated charge at -0.69 V (green line) vs Ag|AgCl from 0.05 M $CuCl_2$: 0.05 M $AuCl_3$ + DES and **(C)** -25 mC of circulated charge at -0.7 V (blue line) vs Ag|AgCl from 0.075 M $CuCl_2$: 0.025 M $AuCl_3$ + DES ; scan rate of 5 mV/s and pH of 3.22.

## 4. Conclusions

We show, for the first time, the preparation of tailored nanostructured bimetallic catalysts of copper and gold, with high active surface area, by metal electrodeposition in a deep eutectic solvent. We show that size, morphology and elemental composition of the deposits can be tailored by selectively adjusting the applied potential and bath composition. The FE-SEM and EDS analysis confirm the formation of nanostructures of either Cu, Au and bimetallic Cu-Au electrodes. Higher Au/Cu ratios in the sample generate rounded gold NPs with similar size (about 200 nm), and with small needles covering the surface. On the other hand, an increased Cu content promotes the development of a network structure with tiny spines. The *ex-situ* XPS analysis confirmed the presence of both Cu and Au in the deposited films, in agreement with the EDS data. Interestingly, it also showed a substantial higher concentration of Cu oxide on the surface compared to Au due to oxidation of the sample by exposure to air.

The ECSA of the prepared nanostructured bimetallic films was estimated by Pb UPD. The current intensity of the Pb UPD considerable increases when the Cu-Au bimetallic nanostructures are deposited on the glassy carbon substrates. An ECSA of 5 to 15 times higher than the geometric active area is estimated by Pb UPD. Thus, we confirm the successful preparation of high surface area nanostructured bimetallic catalysts of Cu and Au, by metal electrodeposition in a deep eutectic solvent. We highlight that the use of green deep eutectic solvents for the sustainable design of bimetallic nanostructured materials is a promising research field for the future design of multimetallic catalysts with high surface area and broad application in electrocatalysis.

*Corresponding author:

E-mail: maria.escudero@chem.ku.dk

E-mail: paula.pascual@chem.ku.dk

ORCID

Paula Sebastián-Pascual: 0000-0001-7985-0750

María Escudero-Escribano: 0000-0002-6432-3015

Kim Nicole Dalby: https://orcid.org/0000-0001-6048-3583

Hanne Falsig:

Ib Chorkendorff: 0000-0003-2738-0325

**Notes**

The authors declare no competing financial interest.

ASSOCIATED CONTENT

Complementary CVs, CAs, FE-SEM images and EDS analysis of pure either Cu and Au electrodeposition in DES are included. Additional FE-SEM and EDS analysis of prepared Cu-Au samples from either the 1:1 or 3:1 molar ratio solution are included. Blank cyclic voltammograms of the Cu-Au samples and Cu and Au polycrystalline electrodes in contact with 0.1M KHCO3 are also included.

ACKNOWLEDGMENT

MEE and PSP gratefully acknowledge the Villum Foundation for financial support through a Villum Young Investigator Grant (project number: 19142). This work was also supported by the Danish foundation through the DFF-Research Project1 (Thematic Research, green transition) grant with number: 0217-00213A; and the DFF-grant Project 1 with number 9041-00224B. We acknowledge support from the Danish National Research Foundation Center for High Entropy Alloy Catalysis (CHEAC, DNRF-149).

## 5. References

(1) Eisenberg, R.; Gray, H. B.; Crabtree, G. W. Addressing the Challenge of Carbon-Free Energy. *Proc. Natl. Acad. Sci. U. S. A.* **2020**, *117* (23), 12543–12549. https://doi.org/10.1073/pnas.1821674116.

(2) De Luna, P.; Hahn, C.; Higgins, D.; Jaffer, S. A.; Jaramillo, T. F.; Sargent, E. H. What Would It Take for Renewably Powered Electrosynthesis to Displace Petrochemical Processes? *Science*. April 2019, p eaav3506. https://doi.org/10.1126/science.aav3506.

(3) Mistry, H.; Varela, A. S.; Kühl, S.; Strasser, P.; Cuenya, B. R. Nanostructured Electrocatalysts with Tunable Activity and Selectivity. *Nat. Rev. Mater.* **2016**, *1* (4), 16009. https://doi.org/10.1038/natrevmats.2016.9.

(4) Sebastián-Pascual, P.; Jordão Pereira, I.; Escudero-Escribano, M. Tailored Electrocatalysts by Controlled Electrochemical Deposition and Surface Nanostructuring. *Chem. Commun.* **2020**, *56* (87), 13261–13272. https://doi.org/10.1039/D0CC06099B.

(5) Trogadas, P.; Ramani, V.; Strasser, P.; Fuller, T. F.; Coppens, M.-O. Hierarchically Structured Nanomaterials for Electrochemical Energy Conversion. *Angew. Chemie Int.*

*Ed.* **2016**, *55* (1), 122–148. https://doi.org/https://doi.org/10.1002/anie.201506394.

(6) Olveira, S.; Forster, S. P.; Seeger, S. Nanocatalysis: Academic Discipline and Industrial Realities. *Hindawi Publ. Corp. J. Nanotechnol.* **2014**, *2014* (Article ID 324089), 1–19. https://doi.org/dx.doi.org/10.1155/2014/324089.

(7) You, H.; Yang, S.; Ding, B.; Yang, H. Synthesis of Colloidal Metal and Metal Alloy Nanoparticles for Electrochemical Energy Applications. *Chem. Soc. Rev.* **2013**, *42* (7), 2880–2904. https://doi.org/10.1039/C2CS35319A.

(8) Li, D.; Wang, C.; Tripkovic, D.; Sun, S.; Markovic, N. M.; Stamenkovic, V. R. Surfactant Removal for Colloidal Nanoparticles from Solution Synthesis: The Effect on Catalytic Performance. *ACS Catal.* **2012**, *2* (7), 1358–1362. https://doi.org/10.1021/cs300219j.

(9) Solla-Gullón, J.; Feliu, J. M. State of the Art in the Electrochemical Characterization of the Surface Structure of Shape-Controlled Pt, Au, and Pd Nanoparticles. *Curr. Opin. Electrochem.* **2020**, *22*, 65–71. https://doi.org/https://doi.org/10.1016/j.coelec.2020.04.010.

(10) Nguyen, M. T.; Yonezawa, T. Sputtering onto a Liquid: Interesting Physical Preparation Method for Multi-Metallic Nanoparticles. *Sci. Technol. Adv. Mater.* **2018**, *19* (1), 883–898. https://doi.org/10.1080/14686996.2018.1542926.

(11) El Abedin, S. Z.; Pölleth, M.; Meiss, S. A.; Janek, J.; Endres, F. Ionic Liquids as Green Electrolytes for the Electrodeposition of Nanomaterials. *Green Chem.* **2007**, *9* (6), 549–555. https://doi.org/10.1039/b614520e.

(12) Tomé, L. I. N.; Baião, V.; da Silva, W.; Brett, C. M. A. Deep Eutectic Solvents for the Production and Application of New Materials. *Appl. Mater. Today* **2018**, *10*, 30–50.

https://doi.org/10.1016/j.apmt.2017.11.005.

(13) Wagle, D. V.; Zhao, H.; Baker, G. A. Deep Eutectic Solvents: Sustainable Media for Nanoscale and Functional Materials. *Acc. Chem. Res.* **2014**, *47* (8), 2299–2308. https://doi.org/10.1021/ar5000488.

(14) Li, C.; Iqbal, M.; Lin, J.; Luo, X.; Jiang, B.; Malgras, V.; Wu, K. C. W.; Kim, J.; Yamauchi, Y. Electrochemical Deposition: An Advanced Approach for Templated Synthesis of Nanoporous Metal Architectures. *Acc. Chem. Res.* **2018**, *51* (8), 1764–1773. https://doi.org/10.1021/acs.accounts.8b00119.

(15) V. S. Protsenko; Danilov, F. I. Current Trends in Electrodeposition of Electrocatalytic Coatings. In *Methods for Electrocatalysis. Springer, Chams*; Inamuddin, Boddula R., A. A., Ed.; 2020.

(16) Gómez, E.; Ramirez, J.; Vallés, E. Electrodeposition of Co-Ni Alloys. *J. Appl. Electrochem.* **1998**, *28* (1), 71–79. https://doi.org/10.1023/A:1003201919054.

(17) Zhang, Q.; De Oliveira Vigier, K.; Royer, S.; Jérôme, F. Deep Eutectic Solvents: Syntheses, Properties and Applications. *Chem. Soc. Rev.* **2012**, *41* (21), 7108–7146. https://doi.org/10.1039/c2cs35178a.

(18) Abbott, A. P.; Boothby, D.; Capper, G.; Davies, D. L.; Rasheed, R. K. Deep Eutectic Solvents Formed between Choline Chloride and Carboxylic Acids: Versatile Alternatives to Ionic Liquids. *J. Am. Chem. Soc.* **2004**, *126* (29), 9142–9147. https://doi.org/10.1021/ja048266j.

(19) Abbott, A. P.; Boothby, D.; Capper, G.; Davies, D. L.; Rasheed, R. K. Deep Eutectic Solvents Formed between Choline Chloride and Carboxylic Acids: Versatile Alternatives

to Ionic Liquids. *J. Am. Chem. Soc.* **2004**, *126* (29), 9142–9147. https://doi.org/10.1021/ja048266j.

(20) Hammons, J. A.; Muselle, T.; Ustarroz, J.; Tzedaki, M.; Raes, M.; Hubin, A.; Terryn, H. Stability, Assembly, and Particle/Solvent Interactions of Pd Nanoparticles Electrodeposited from a Deep Eutectic Solvent. *J. Phys. Chem. C* **2013**, *117* (27), 14381–14389. https://doi.org/10.1021/jp403739y.

(21) Sebastián, P.; Giannotti, M. I.; Gómez, E.; Feliu, J. M. Surface Sensitive Nickel Electrodeposition in Deep Eutectic Solvent. *ACS Appl. Energy Mater.* **2018**, *1* (3), 1016–1028. https://doi.org/10.1021/acsaem.7b00177.

(22) Sebastián, P.; Vallés, E.; Gómez, E. First Stages of Silver Electrodeposition in a Deep Eutectic Solvent. Comparative Behavior in Aqueous Medium. *Electrochim. Acta* **2013**, *112*, 149–158. https://doi.org/10.1016/J.ELECTACTA.2013.08.144.

(23) Sebastián, P.; Vallés, E.; Gómez, E. Copper Electrodeposition in a Deep Eutectic Solvent. First Stages Analysis Considering Cu(I) Stabilization in Chloride Media. *Electrochim. Acta* **2014**, *123*, 285–295. https://doi.org/10.1016/J.ELECTACTA.2014.01.062.

(24) Wei, L.; Lu, B.; Sun, M.; Tian, N.; Zhou, Z.; Xu, B.; Zhao, X.; Sun, S. Overpotential-Dependent Shape Evolution of Gold Nanocrystals Grown in a Deep Eutectic Solvent. *Nano Res.* **2016**, *9* (11), 3547–3557. https://doi.org/10.1007/s12274-016-1236-1.

(25) Abbott, A. P.; Alhaji, A. I.; Ryder, K. S.; Horne, M.; Rodopoulos, T. Electrodeposition of Copper–Tin Alloys Using Deep Eutectic Solvents. *Trans. IMF* **2016**, *94* (2), 104–113. https://doi.org/10.1080/00202967.2016.1148442.

(26) Kumar-Krishnan, S.; Esparza, R.; Pal, U. Controlled Fabrication of Flower-Shaped Au–

Cu Nanostructures Using a Deep Eutectic Solvent and Their Performance in Surface-Enhanced Raman Scattering-Based Molecular Sensing. *ACS Omega* **2020**, *5* (7), 3699–3708. https://doi.org/10.1021/acsomega.9b04355.

(27) Guillamat, P.; Cortés, M.; Vallés, E.; Gómez, E. Electrodeposited CoPt Films from a Deep Eutectic Solvent. *Surf. Coatings Technol.* **2012**, *206* (21), 4439–4448. https://doi.org/https://doi.org/10.1016/j.surfcoat.2012.04.093.

(28) Manolova, M.; Böck, R.; Scharf, I.; Mehner, T.; Lampke, T. Electrodeposition of Pd Alloys from Choline Chloride/Urea Deep Eutectic Solvents. *J. Alloys Compd.* **2021**, *855*, 157462. https://doi.org/https://doi.org/10.1016/j.jallcom.2020.157462.

(29) Liu, A.; Shi, Z.; Reddy, R. G. Mechanism Study of Cu-Zn Alloys Electrodeposition in Deep Eutectic Solvents. *Ionics (Kiel).* **2020**, *26* (6), 3161–3172. https://doi.org/10.1007/s11581-019-03418-2.

(30) Tian, N.; Xiao, J.; Zhou, Z.-Y.; Liu, H.-X.; Deng, Y.-J.; Huang, L.; Xu, B.-B.; Sun, S.-G. Pt-Group Bimetallic Nanocrystals with High-Index Facets as High Performance Electrocatalysts. *Faraday Discuss.* **2013**, *162* (0), 77–89. https://doi.org/10.1039/C3FD20146E.

(31) Tian, N.; Lu, B.-A.; Yang, X.-D.; Huang, R.; Jiang, Y.-X.; Zhou, Z.-Y.; Sun, S.-G. Rational Design and Synthesis of Low-Temperature Fuel Cell Electrocatalysts. *Electrochem. Energy Rev.* **2018**, *1* (1), 54–83. https://doi.org/10.1007/s41918-018-0004-1.

(32) García-Cruz, L.; Montiel, V.; Solla-Gullón, J. Shape-Controlled Metal Nanoparticles for Electrocatalytic Applications. *Phys. Sci. Rev.* **2018**, *4* (1), 20170124. https://doi.org/https://doi.org/10.1515/psr-2017-0124.

(33) Wu, Z.-P.; Shan, S.; Zang, S.-Q.; Zhong, C.-J. Dynamic Core–Shell and Alloy Structures of Multimetallic Nanomaterials and Their Catalytic Synergies. *Acc. Chem. Res.* **2020**. https://doi.org/10.1021/acs.accounts.0c00564.

(34) Pedersen, J. K.; Batchelor, T. A. A.; Bagger, A.; Rossmeisl, J. High-Entropy Alloys as Catalysts for the CO2 and CO Reduction Reactions. *ACS Catal.* **2020**, *10* (3), 2169–2176. https://doi.org/10.1021/acscatal.9b04343.

(35) Chen, C.; Kang, Y.; Huo, Z.; Zhu, Z.; Huang, W.; Xin, H. L.; Snyder, J. D.; Li, D.; Herron, J. A.; Mavrikakis, M.; Chi, M.; More, K. L.; Li, Y.; Markovic, N. M.; Somorjai, G. A.; Yang, P.; Stamenkovic, V. R. Highly Crystalline Multimetallic Nanoframes with Three-Dimensional Electrocatalytic Surfaces. *Science* **2014**, *343* (6177), 1339–1343. https://doi.org/10.1126/science.1249061.

(36) Liu, P.; Nørskov, J. K. Ligand and Ensemble Effects in Adsorption on Alloy Surfaces. *Phys. Chem. Chem. Phys.* **2001**, *3* (17), 3814–3818. https://doi.org/10.1039/b103525h.

(37) Fiuza, T. E. R.; Zanchet, D. Supported AuCu Alloy Nanoparticles for the Preferential Oxidation of CO (CO-PROX). *ACS Appl. Nano Mater.* **2020**, *3* (1), 923–934. https://doi.org/10.1021/acsanm.9b02596.

(38) Liu, M.; Zhou, W.; Wang, T.; Wang, D.; Liu, L.; Ye, J. High Performance Au–Cu Alloy for Enhanced Visible-Light Water Splitting Driven by Coinage Metals. *Chem. Commun.* **2016**, *52* (25), 4694–4697. https://doi.org/10.1039/C6CC00717A.

(39) Wang, J.; Zhu, H.; Yu, D.; Chen, J.; Chen, J.; Zhang, M.; Wang, L.; Du, M. Engineering the Composition and Structure of Bimetallic Au–Cu Alloy Nanoparticles in Carbon Nanofibers: Self-Supported Electrode Materials for Electrocatalytic Water Splitting. *ACS*

*Appl. Mater. Interfaces* **2017**, *9* (23), 19756–19765. https://doi.org/10.1021/acsami.7b01418.

(40) Liu, D.; Luo, Q.; Zhou, F. Nonenzymatic Glucose Sensor Based on Gold–Copper Alloy Nanoparticles on Defect Sites of Carbon Nanotubes by Spontaneous Reduction. *Synth. Met.* **2010**, *160* (15), 1745–1748. https://doi.org/https://doi.org/10.1016/j.synthmet.2010.06.011.

(41) Morales-Guio, C. G.; Cave, E. R.; Nitopi, S. A.; Feaster, J. T.; Wang, L.; Kuhl, K. P.; Jackson, A.; Johnson, N. C.; Abram, D. N.; Hatsukade, T.; Hahn, C.; Jaramillo, T. F. Improved CO2 Reduction Activity towards C2+ Alcohols on a Tandem Gold on Copper Electrocatalyst. *Nat. Catal.* **2018**, *1* (10), 764–771. https://doi.org/10.1038/s41929-018-0139-9.

(42) Shen, S.; Peng, X.; Song, L.; Qiu, Y.; Li, C.; Zhuo, L.; He, J.; Ren, J.; Liu, X.; Luo, J. AuCu Alloy Nanoparticle Embedded Cu Submicrocone Arrays for Selective Conversion of CO2 to Ethanol. *Small* **2019**, *15* (37), 1902229. https://doi.org/https://doi.org/10.1002/smll.201902229.

(43) Liu, K.; Ma, M.; Wu, L.; Valenti, M.; Cardenas-Morcoso, D.; Hofmann, J. P.; Bisquert, J.; Gimenez, S.; Smith, W. A. Electronic Effects Determine the Selectivity of Planar Au–Cu Bimetallic Thin Films for Electrochemical CO2 Reduction. *ACS Appl. Mater. Interfaces* **2019**, *11* (18), 16546–16555. https://doi.org/10.1021/acsami.9b01553.

(44) Kim, D.; Resasco, J.; Yu, Y.; Asiri, A. M.; Yang, P. Synergistic Geometric and Electronic Effects for Electrochemical Reduction of Carbon Dioxide Using Gold–Copper Bimetallic Nanoparticles. *Nat. Commun.* **2014**, *5*, 4948.

(45) Li, G. R.; Xu, H.; Lu, X. F.; Feng, J. X.; Tong, Y. X.; Su, C. Y. Electrochemical Synthesis of Nanostructured Materials for Electrochemical Energy Conversion and Storage. *Nanoscale* **2013**, *5* (10), 4056–4069. https://doi.org/10.1039/c3nr00607g.

(46) Tang, W.; Peterson, A. A.; Varela, A. S.; Jovanov, Z. P.; Bech, L.; Durand, W. J.; Dahl, S.; Nørskov, J. K.; Chorkendorff, I. The Importance of Surface Morphology in Controlling the Selectivity of Polycrystalline Copper for CO2 Electroreduction. *Phys. Chem. Chem. Phys.* **2012**, *14* (1), 76–81. https://doi.org/10.1039/C1CP22700A.

(47) Koper, M. T. M. Structure Sensitivity and Nanoscale Effects in Electrocatalysis. *Nanoscale* **2011**, *3* (5), 2054–2073. https://doi.org/10.1039/c0nr00857e.

(48) Bentley, C. L.; Kang, M.; Unwin, P. R. Nanoscale Surface Structure–Activity in Electrochemistry and Electrocatalysis. *J. Am. Chem. Soc.* **2019**, *141* (6), 2179–2193. https://doi.org/10.1021/jacs.8b09828.

(49) Menzel, N.; Ortel, E.; Kraehnert, R.; Strasser, P. Electrocatalysis Using Porous Nanostructured Materials. *ChemPhysChem* **2012**, *13* (6), 1385–1394. https://doi.org/https://doi.org/10.1002/cphc.201100984.

(50) Sievers, G. W.; Jensen, A. W.; Quinson, J.; Zana, A.; Bizzotto, F.; Oezaslan, M.; Dworzak, A.; Kirkensgaard, J. J. K.; Smitshuysen, T. E. L.; Kadkhodazadeh, S.; Juelsholt, M.; Jensen, K. M. Ø.; Anklam, K.; Wan, H.; Schäfer, J.; Čépe, K.; Escudero-Escribano, M.; Rossmeisl, J.; Quade, A.; Brüser, V.; Arenz, M. Self-Supported Pt–CoO Networks Combining High Specific Activity with High Surface Area for Oxygen Reduction. *Nat. Mater.* **2020**. https://doi.org/10.1038/s41563-020-0775-8.

(51) Chen, Q.-S.; Vidal-Iglesias, F. J.; Solla-Gullón, J.; Sun, S.-G.; Feliu, J. M. Role of Surface

Defect Sites: From Pt Model Surfaces to Shape-Controlled Nanoparticles. *Chem. Sci.* **2012**, *3* (1), 136–147. https://doi.org/10.1039/C1SC00503K.

(52) Jensen, A. W.; Sievers, G. W.; Jensen, K. D.; Quinson, J.; Arminio-Ravelo, J. A.; Brüser, V.; Arenz, M.; Escudero-Escribano, M. Self-Supported Nanostructured Iridium-Based Networks as Highly Active Electrocatalysts for Oxygen Evolution in Acidic Media. *J. Mater. Chem. A* **2020**, *8* (3), 1066–1071. https://doi.org/10.1039/C9TA12796H.

(53) Landa-Castro, M.; Sebastián, P.; Giannotti, M. I.; Serrà, A.; Gómez, E. Electrodeposition of Nanostructured Cobalt Films from a Deep Eutectic Solvent: Influence of the Substrate and Deposition Potential Range. *Electrochim. Acta* **2020**, 136928. https://doi.org/https://doi.org/10.1016/j.electacta.2020.136928.

(54) Smith, E. L.; Abbott, A. P.; Ryder, K. S. Deep Eutectic Solvents (DESs) and Their Applications. *Chem. Rev.* **2014**, *114* (21), 11060–11082. https://doi.org/10.1021/cr300162p.

(55) Garnier, E.; Vidal-Iglesias, F. J.; Feliu, J. M.; Solla-Gullón, J. Surface Structure Characterization of Shape and Size Controlled Pd Nanoparticles by Cu UPD: A Quantitative Approach. *Front. Chem.* **2019**, *7*, 527. https://doi.org/10.3389/fchem.2019.00527.

(56) Clavilier, J. The Role of Anion on the Electrochemical Behaviour of a (111) Platinum Surface, An Unusual Splitting of the Voltammogram in the Hydrogen Region. *J Electroanal Chem* **1980**, *107*, 211–216. https://doi.org/10.1016/S0022-0728(79)80023-6.

(57) Zhang, Q. B.; Hua, Y. X. Electrochemical Synthesis of Copper Nanoparticles Using Cuprous Oxide as a Precursor in Choline Chloride-Urea Deep Eutectic Solvent:

Nucleation and Growth Mechanism. *Phys. Chem. Chem. Phys.* **2014**, *16* (48), 27088–27095. https://doi.org/10.1039/c4cp03041a.

(58) Sebastián, P.; Torralba, E.; Vallés, E.; Molina, A.; Gómez, E. Advances in Copper Electrodeposition in Chloride Excess. A Theoretical and Experimental Approach. *Electrochim. Acta* **2015**, *164*, 187–195. https://doi.org/10.1016/j.electacta.2015.02.206.

(59) Trasatti, S.; Petrii, O. A. Real Surface Area Measurements in Electrochemistry. *J. electroanal. chem* **1992**, *327* (1–2), 353–376. https://doi.org/10.1016/0926-860X(96)80148-7.

(60) Li, D.; Batchelor-McAuley, C.; Compton, R. G. Some Thoughts about Reporting the Electrocatalytic Performance of Nanomaterials. *Appl. Mater. Today* **2020**, *18*, 100404. https://doi.org/https://doi.org/10.1016/j.apmt.2019.05.011.